51st AIAA Aerospace Sciences Meeting including the New Horizons Forum and Aerospace Exposition
07 - 10 January 2013, Grapevine (Dallas/Ft. Worth Region), Texas

AIAA 2013-0245

Study of a Swept Wing with Leading-Edge Ice Using a Wake Survey Technique

Jeff M. Diebold* and Michael B. Bragg†
University of Illinois at Urbana-Champaign, Urbana, IL 61801

The aerodynamics of swept wings with leading-edge ice is very complex and not fully understood. Previous swept wing icing studies have only provided force balance measurements and/or qualitative flow visualization. In order to more fully understand the complex aerodynamics it is necessary to understand how the ice influences the drag breakdown and the spanwise distributions of lift and drag. This paper utilizes 5-hole probe wake surveys and a far-field analysis to decompose the drag into profile and induced drag components and to determine the spanwise distributions of lift and drag. It is shown that the leading-edge ice primarily influences the profile drag and the induced drag is relatively unaltered. Features observed in the lift and drag distributions are related to features seen in the wake as well as in surface oil flow visualization.

Nomenclature

$c(y)$	=	Chord distribution
C_d	=	Sectional total drag coefficient
C_{di}	=	Sectional induced drag coefficient
C_{dp}	=	Sectional profile drag coefficient
C_l	=	Sectional lift coefficient
C_D	=	Total Drag coefficient
C_{Di}	=	Induced drag coefficient
C_L	=	Lift coefficient
D	=	Total Drag
D_i	=	Induced drag
D_p	=	Profile drag
L	=	Lift
P	=	Static pressure
P_t	=	Total pressure in the wake
$P_{t\infty}$	=	Freestream total pressure
u	=	Streamwise velocity in the wake
u_b	=	Wake blockage velocity
u'	=	Perturbation velocity
u^*	=	Artificial velocity
U_∞	=	Freestream velocity
v	=	Spanwise velocity in the wake
w	=	Normal velocity in the wake
x	=	Streamwise direction
y	=	Spanwise direction (positive from root to tip)
z	=	Normal direction (positive from lower to upper surface)
α	=	Model angle of attack (measured at the root)
ψ	=	Stream function in the transverse plane
ξ	=	Streamwise vorticity

* Graduate Research Assistant, Department of Aeronautical and Astronautical Engineering, Member AIAA
† Professor of Aerospace Engineering, Interim Dean of College of Engineering, Fellow AIAA

1.0 Introduction

It is well known that the presence of ice on aerodynamic surfaces can significantly impact the performance of an aircraft.[1] A considerable amount of effort has been spent gaining an understanding of the aerodynamic impact of ice accretion on airfoils.[2,3] Over the past several years however there has been an increased interest in the effect of ice on swept wings. Papadakis et. al.[4] studied the aerodynamic performance of a swept wing with ice accretions formed in NASA's Icing Research Tunnel.[5] The wind tunnel model had a leading-edge sweep angle of 28 deg. and an aspect ratio of 6.8. Measured lift coefficients decreased by nearly 40% with accompanying minimum drag increases of 1200% for certain ice shapes. In addition, Papadakis et. al.[6] investigated the effects of two simulated ice shapes on the performance of a T-Tail with a leading-edge sweep angle of 29 deg. and an aspect ratio of 4.4. The simulated ice shapes were tested with and without roughness. The maximum decrease in lift ranged from 10 – 40% with drag increases ranging from 86 – 236% for the various configurations tested. More recently, Broeren et. al.[7] investigated the effects of various ice simulations on the aerodynamics of a generic transport aircraft. In addition to the performance measurements, surface oil flow visualization was used to study the flowfield induced by the ice. The flow visualization indicated regions of separated and reversed flow forming a spanwise running leading-edge vortex similar to the leading-edge vortex seen by Bragg and Khodadoust[8] when using LDV to study the flowfield of a swept NACA 0012 with a simulated ice shape. Finally, Diebold et. al.[9] investigated the effects of a simulated ice shape on the performance and flowfield of the swept wing used for this paper. They used several techniques including force balance measurements, surface oil flow visualization, pressure sensitive paint and qualitative five-hole probe wake surveys.

The effects of ice on a swept wing are highly complex and provide measurement challenges and opportunities that were not available when testing airfoils. Measurements in the wake of a three dimensional wing using a five-hole probe (5HP) or similar device can provide a significant amount of information not easily obtainable through other means. By measuring total and static pressure as well as all three components of velocity in the wake it is possible to obtain not only the total lift and drag but also the spanwise distributions of these quantities and the drag can be decomposed into profile and induced drag components. This information cannot be determined from a force balance and can prove valuable when trying to better understand the performance effects of the ice. Hackett and Sugavanam[10] used a 5HP to measure the drag of a car and a stalled straight wing. For the stalled wing they showed that profile drag accounted for 80% of the total drag while induced or vortex drag made up the remainder. Brune[11] made measurements in the wake of a simple rectangular NACA 0016 wing with an aspect ratio of 6. At an angle of attack of 8.2º profile and induced drag accounted for 46 and 54% of the total drag, respectively. Brune also presented spanwise distributions of profile and induced drag and it was seen that in both cases the maximum sectional drag coefficient occurred at the tips. The maximum induced drag coefficient occurs at the tips due to the high level of vorticity in the tip vortex, and the maximum profile drag coefficient occurs at the tips due to the high axial velocity deficit within the vortex core; however, when there are large regions of separated flow, the maximum profile drag may occur elsewhere along the span. Kusunose[12] analyzed previously acquired wake survey data, including the data of Brune,[11] using a variety of methods to reduce the data.

Iced swept wing aerodynamics is complex and not fully understood. Force balance measurements only provide total lift and drag and no information about the different drag components or the spanwise variation in lift and drag. Flow visualization can only provide qualitative information regarding the spanwise variation in performance. The goal of this paper is to use 5HP wake surveys in order to better understand how the ice influences the aerodynamic performance of a swept wing by investigating the effects on the different drag components and the spanwise distributions of lift and drag. Global and local changes in performance will be related to observed features in the flowfield.

2.0 Wake Survey Analysis

By analyzing the control volume shown in Fig. 1 the following expressions for lift and drag can be derived, as shown in Brune.[11] Note that lift is in the positive z-direction.

$$L = \iint_{Side\ wall\ z-} P\,dxdy \;-\; \iint_{Side\ wall\ z+} P\,dxdy \;-\; \rho \iint_{S_2} uw\,dydz \tag{1}$$

$$D = \iint_w \left((P_{t\infty} - P_t)\right) dydz \;+\; \frac{\rho}{2}\iint_{S_2} (U_\infty^2 - u^2)\,dydz + \frac{\rho}{2}\iint_{S_2} (v^2 - w^2)\,dydz \tag{2}$$

While these two expressions are exact, they are not practical from an experimental point of view. Calculating the lift requires integrating the pressure over the sidewalls, and both expressions contain integrals that must be performed over the entire downstream plane S_2. A practical set of equations will consist only of wake integrals such as the first integral in Eq. 2, where outside of the wake $P_t = P_{t\infty}$ and the integrand is zero.

A detailed derivation of the wake survey equations used in this paper will not be given but can be found in numerous sources.[10,11,12] The derivation follows the work of Betz[13] and Maskell[14] and the final expressions are given here. The final expressions for lift and drag require measurements of the pressure and velocity components in the viscous wake.

One of the main advantages of the wake survey as opposed to force balance measurements is the ability to decompose drag into profile and induced drag components. The wake integral expressions for the two components of drag are given by Eqs. 3 and 4.

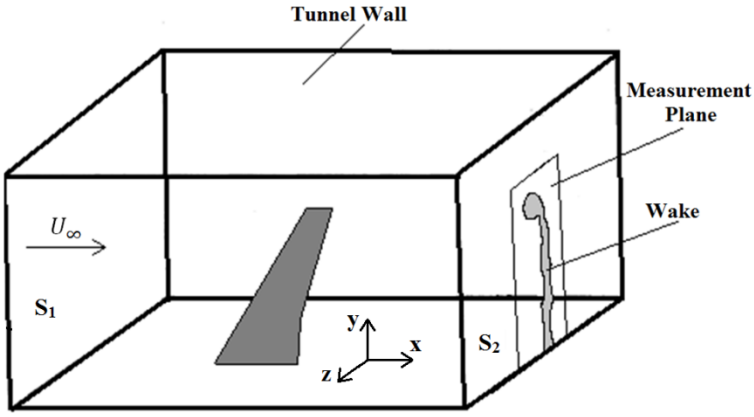

Fig. 1 Control volume and coordinate system used in wake survey.

$$D_p = \iint_w \left((P_{t\infty} - P_t) + \frac{\rho}{2}(u - u^*)\big(u + u^* - 2(U_\infty + u_b)\big)\right) dydz \tag{3}$$

$$D_i = \frac{\rho}{2}\iint_w \psi\xi\,dydz \tag{4}$$

The total drag was the sum of the profile and induced drag components. In Eq. 3, u^* and u_b are known as the artificial velocity and wake blockage velocity, respectively. The artificial velocity was introduced by Betz[13] and is defined in Eq. 5. Notice the artificial velocity is equal to the freestream velocity outside of the viscous wake.

$$u^{*2} = u^2 + {}^2/_\rho\,(P_{t\infty} - P_t) \tag{5}$$

The wake blockage velocity was interpreted by Maskell[14] as a small correction due to the effect of tunnel walls.

$$u_b = \frac{1}{2S_2}\iint_W (u^* - u)\,dydz \tag{6}$$

The profile drag only requires measurements of the total pressure and axial velocity within the wake, outside of the wake the integrand is zero.

In Eq. 4, for the induced drag, ξ and ψ are the streamwise vorticity and the transverse stream function, respectively. The vorticity is defined as:

$$\xi = \frac{\partial w}{\partial y} - \frac{\partial v}{\partial z} \tag{7}$$

The transverse stream function ψ satisfies the following Poisson equation.

$$\frac{\partial^2\psi}{\partial y^2} + \frac{\partial^2\psi}{\partial z^2} = -\xi \tag{8}$$

Requiring the tunnel wall to be a streamline in the transverse plane provides the following boundary conditions for ψ on the tunnel walls.

$$(\psi)_{wall} = 0 \tag{9}$$

Equation 4 for the induced drag is a wake integral, because the vorticity (ξ) is zero outside of the wake.
The lift is given by the following expression, where y is the distance measured from the tunnel floor.

$$L = \rho \iint_W \; y\xi \; dydz \tag{10}$$

The sectional lift coefficient can be determined by assuming a planar wake and applying the Kutta-Joukowski theorem.[12]

$$C_l(y) = \frac{2}{U_\infty c(y)} \int_{b/2}^{y} \int_w \; \xi(y,z)\, dz\, dy \tag{11}$$

Where c(y) is the local chord measured in the streamwise direction. The integrands of Eqs. 10 and 11 are zero outside of the wake.

3.0 Experimental Methods

This section will discuss the relevant experimental techniques used in this study. The model and ice shape simulation are described in Diebold et. al.[9] and will therefore only be briefly discussed here.

3.1 Wind Tunnel

Wind tunnel tests were performed in the University of Illinois subsonic wind tunnel. The wind tunnel is of the open-return type with a rectangular test section measuring 2.8-ft by 4-ft. The maximum speed in the empty test section was approximately 165 mph (242 ft/s), this corresponds to a Reynolds number of 1.5×10^6/ft. The turbulence intensity in the test section was approximately 0.1% over the entire operating range.

3.2 Model

For this study a modified version of the Common Research Model (CRM) was used. The CRM was designed by Vassberg et. al.[15] for the 4th AIAA Drag Prediction Workshop. It was chosen for the original swept wing icing study by Diebold et. al.[9] because in addition to representing the wing of a modern commercial airliner, the full geometry as well as experimental and computational data are publicly available. The model used at the University of Illinois was of the reflection plane type and is shown in Fig. 2. The geometry was modified slightly from the original CRM to ease construction; these modifications are discussed in Diebold et. al.[9] The relevant geometric parameters are given Table 1.

Fig. 2 Wind tunnel model.

Table 1 Geometric features of the swept wing model.

AR	LE Sweep	MAC (ft)	Semispan (ft)	Taper Ratio
8.3	35°	0.5817	2.1	0.296

The model was supported by an internal steel frame and three rapid prototyped components formed the skin. The three components were the upper and lower surface and a removable leading-edge. Two leading-edges were built, a clean leading-edge and an iced leading-edge. The leading-edge piece was easily removed so that it was possible to quickly switch between the two. It should be noted that the model used in this study is not the same model used by Diebold et. al.[9] The original model had minor surface quality problems primarily due to warping of the outer skin. The internal structure of the rapid prototyped components was redesigned to improve the surface quality and a second model was constructed. As a result, the data presented in the original reference[9] is not directly applicable here because the models were not identical; however, all of the observed trends are the same. While the new model is a significant improvement over the original there are still some minor flaws where the leading-edge component meets the upper surface components.

3.3 Ice Shape Simulation

The ice shape used in this study was a simple simulation developed using 2D strip theory discussed by Potapczuk et. al.[16] Several spanwise locations, normal to the leading-edge, along the wing were chosen and at each location a two dimensional ice accretion was generated for the local airfoil using NASA's LEWICE 3.0. The resulting series of two dimensional ice shapes were blended along the span of the wing and the full three dimensional ice shape was then built as part of the removable leading-edge. The icing conditions were chosen to produce a reasonably sized ice shape. A more detailed description of the exact procedure used is given by Diebold.[17] The conditions input into LEWICE are listed in Table **2**, and ice shape cross-sections near the root, midspan and tip are shown in Fig. 3. It should be noted in Fig. 3, the coordinates are non-dimensionalized by the local chord, and therefore it can be seen that the size of the ice shape relative to the local chord increases significantly from root to tip.

Table 2 Icing conditions used to generate ice shape simulation.

Time (sec)	V_∞ (mph)	LWC (g/m^3)	δ (μm)	Temp (F)
2400	205	1	30	20

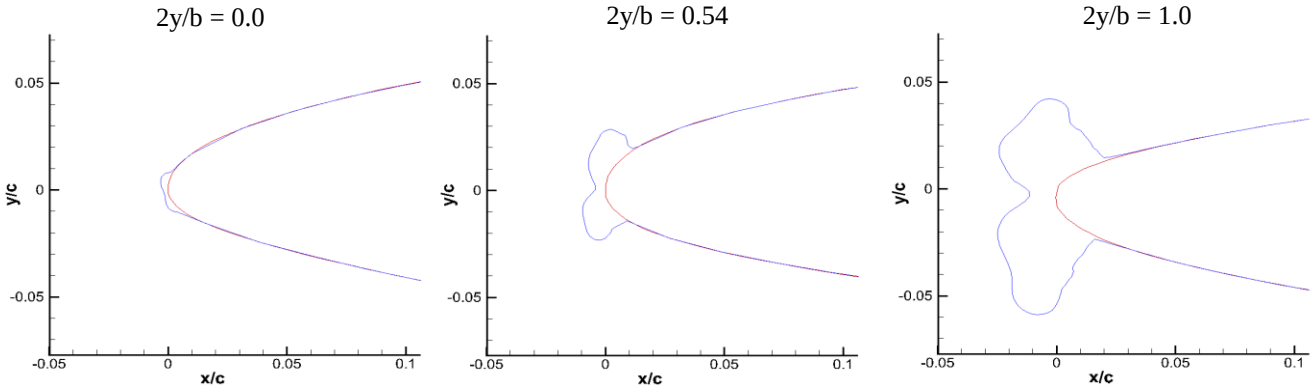

Fig. 3 Ice shape cross-section at several spanwise locations.

3.4 Wake Survey

The five-hole probe (5HP) used in this study was an Aeroprobe Corp., model PS5-C318-152. The diameter of the probe tip was 0.125-inches. The probe was traversed through a plane located at 2x/b = 0.8 downstream of the trailing-edge of the tip. The survey extended from approximately 2y/b = 0.10 to 2y/b = 1.05 in the spanwise direction. The survey region in the z-direction varied for each case and was chosen to minimize the wake survey time by only taking measurements in the wake. The survey area captured the entire wake except for the portion of the span from the root to approximately 2y/b = 0.10. This region was avoided due to the influence of the floor boundary layer. A variable step size was used depending on where the probe was located. Below the tip vortex region the stepsize in the z-direction was 0.125 inches ($2\Delta z/b = 0.0049$) and in the spanwise direction 0.25 inches ($2\Delta y/b = 0.0099$). In the vicinity of the tip vortex (approximately 2y/b > 0.93) the stepsize was 0.125 inches in both directions.

All measurements were made at a Reynolds number of 6×10^5 based on the mean aerodynamic chord of the model. For the clean wing, wake surveys were performed from $\alpha = 2^\circ$ to 10° and for the iced wing $\alpha = 2^\circ$ to 6°. The calibration procedure and data reduction process used in this study are described in Diebold.[17] A basic overview of

the data reduction process is given here. After the measurements were made the calibration was applied to determine the total and static pressure as well as all three components of velocity. The data were then interpolated onto an evenly space grid with a stepsize of 0.125 inches. The velocity was used to calculate the vorticity using a second order finite differencing method. Ideally the vorticity and total pressure loss would both be zero outside of the viscous wake; however, due to random measurement error this was not the case and it was necessary to identify the viscous wake region in the measurement plane. The edge of the wake was found for each spanwise location by determining where the derivative of the total pressure loss with respect to the z-coordinate exceeded a certain threshold. This method was very effective at identifying the edge of the wake, and the final result was not significantly sensitive to the value of the threshold used.[17]

With the wake region identified the integrations in the lift and drag equations could be performed over the wake. The axial velocity and total pressure loss were used to calculate the profile drag using Eq. 3, and the lift was calculated using Eq. 10. The boundary condition for the Poisson equation, Eq. 8, must be applied on the tunnel walls. The computational domain was extended to the side walls and the ceiling of the tunnel; however, since no measurements were made below 2y/b = 0.10 the boundary condition was applied directly to this edge of the measurement plane. Note that outside of the wake, Eq. 8 reduces to Laplace's Equation because $\xi = 0$. See Diebold[17] for a discussion of the numerical method used to solve Eq. 8. Finally, the induced drag is calculated from Eq. 4. The lift and drag calculated from the wake survey data was corrected for tunnel wall effects using the same procedure as for the force balance measurements.[17]

4.0 Results and Discussion

Before presenting the wake survey results the general flowfields of the clean and iced wing will be briefly discussed. As mentioned above, the model used in this study is an improved version of the model used by Diebold et. al.[9] The geometry was the same but the surface quality of the model used for this paper was improved. Since the models were not the same, the data presented here is not identical to the previous data; however, many of the trends of flowfield features are the same. Therefore only a brief discussion of the flowfield will be given and more detail can be found in Diebold et. al.[9] and Diebold.[17]

The surface oil flow results for the clean wing at Re = $6x10^5$ for several angles of attack are shown in Fig. 4. It should be noted the bright streaks seen at roughly 30% and 70% semispan were due to small imperfections where the removable leading-edge met the upper surface. There are several important flowfield features seen in the oil. First, as the angle of attack increased the oil flow indicated increasing spanwise flow along the surface due to the increasing strength of the spanwise pressure gradient resulting from the wing sweep. Beginning at $\alpha = 4.4^o$ an oil accumulation line was seen near the leading-edge running along most of the span. This line indicated flow separation and the formation of a small leading-edge vortex; this is similar to a laminar separation bubble on an airfoil but the vortex is three dimensional. The clean wing stalled as a result of the flow on the outboard sections failing to reattach. The separated shear layer rolled up to form a large leading-edge vortex that was shed into the wake, this flowfield is seen in the image for $\alpha = 10.7^o$. The flow on the inboard sections of the wing remained attached while outboard of the leading-edge vortex the flow on the surface is reversed and these sections are stalled.

The flowfield images for the iced wing are shown in Fig. 5. The flowfield of the iced wing was substantially different due to flow separation from the tip of the ice shape. Below stall, the separated shear layer rolled up to form a leading-edge vortex that reattached to the surface of the wing along the entire span. In Fig. 5, the reattachment line of the vortex has been highlighted. As the angle of attack increased the size of the leading-edge vortex increased. This was very similar to the behavior of a separation bubble behind a horn ice on an airfoil. The leading-edge vortex continued to increase until if failed to reattach along the outer sections of the wing as seen at $\alpha = 6.5^o$. The surface oil flow of the stalled iced wing was similar to that of the stalled clean wing; the flow on the inboard sections was still attached while the outboard sections were stalled. The structure of the leading-edge vortex is described in more detail by Diebold et. al.[9] An important feature to notice is that in general, the size of the leading-edge vortex relative to the local chord increased along the span. This was very noticeable at $\alpha = 5.5^o$, where the flow quickly reattached behind the ice shape near the root, but in the tip region the leading-edge vortex occupied nearly the entire chord. The significance of this observation will be discussed below.

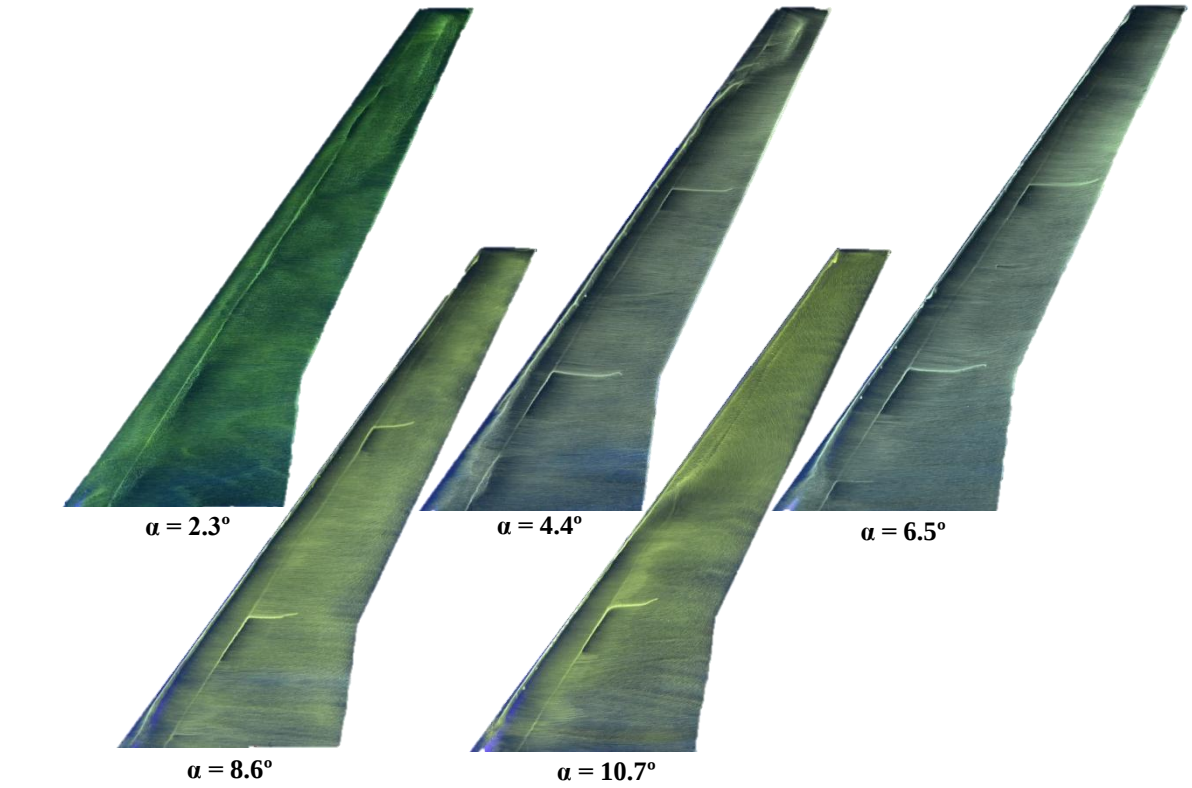

Fig. 4 Surface oil flow for the clean wing at several angles of attack. Re = 6x10^5

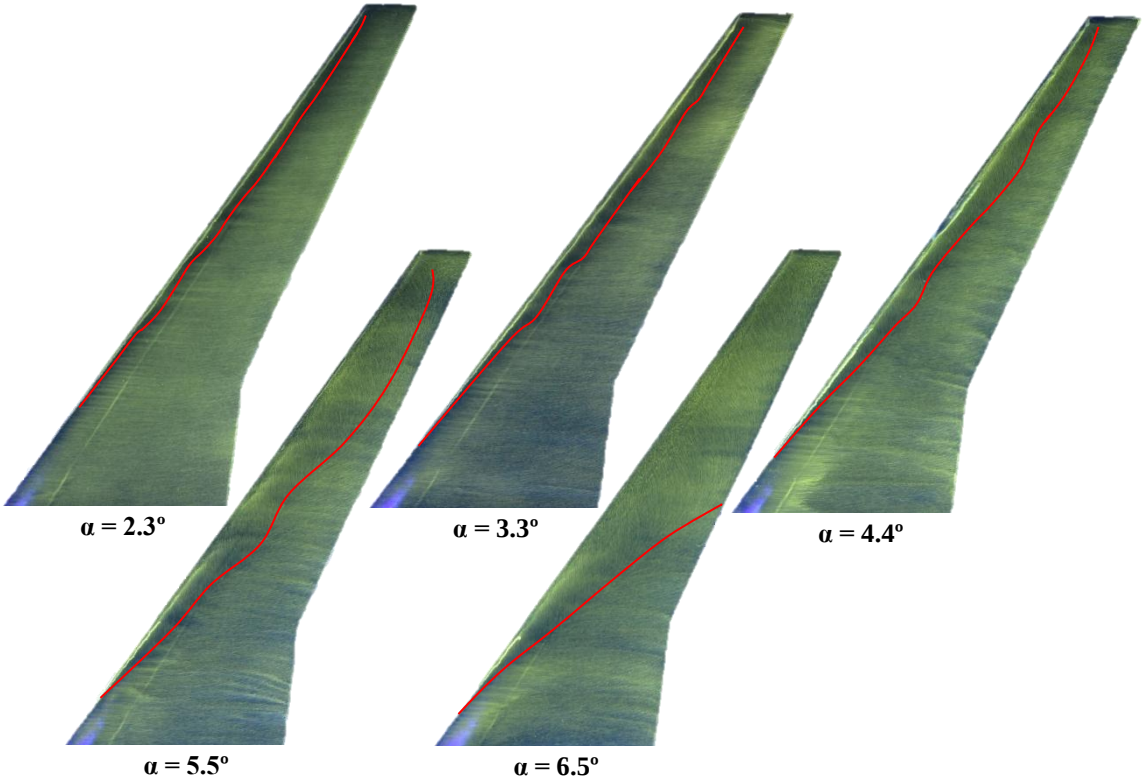

Fig. 5 Surface oil flow for the iced wing at several angles of attack, with the reattachment line highlighted. Re = 6x10^5

Figure 6 compares the total lift and drag measured by the force balance and wake survey for the clean and iced wing at Re = $6x10^5$. Comparing the force balance data of the clean and iced wing it can be seen that below stall the ice caused a small decrease in lift for a given angle of attack and a significant increase in drag. The increase in the minimum drag coefficient due to the ice was 81.1% while at a lift coefficient of 0.5 the increase in the drag coefficient was 69.7%. The clean wing stalled at an angle of attack of approximately 9.7º while the iced wing stalled at approximately 6.0º. The ice significantly changed the behavior of the lift curve after stall. For the clean wing the lift was nearly constant after stall, but the lift of the iced wing continued to increase but the slope was reduced.

Comparing the force balance measurements and the wake survey results it can be seen that the wake survey method was able to accurately determine the lift and drag. The average error, relative to the balance, in the lift calculated from the wake data was 3.05% and 2.3% for the clean and iced wing, respectively. For the drag, the average error was 14.6% and 13.3% for the clean and iced wing, respectively. While the error in the drag was relatively large, it can be seen in Fig. 6b that the drag curve determined from the wake survey follow the curve from the force balance measurements very well, but the wake survey consistently under predicted the drag. A possible explanation for this was that the inboard 10% of the wake was not surveyed and therefore the drag contribution from this region would not have been captured. Overall the wake survey was able to accurately capture both the lift and drag including the effects of stall.

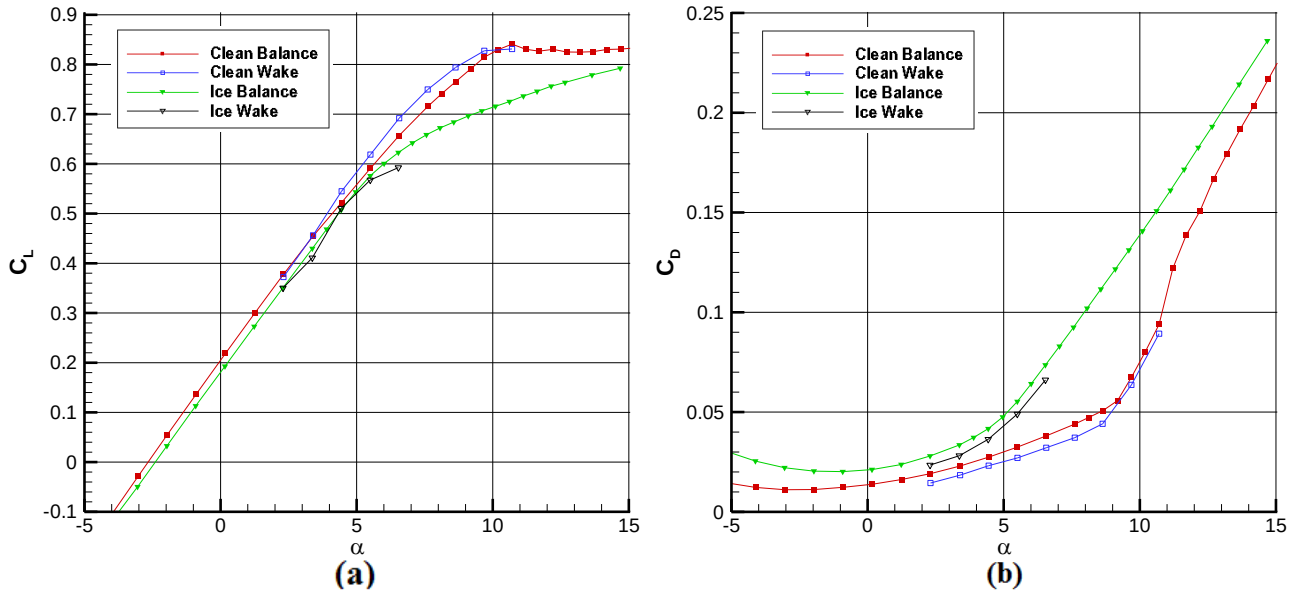

Fig. 6 Comparison of lift (a) and drag (b) from the balance and wake. Re = $6x10^5$

Figure 7 shows the lift coefficient versus the decomposed profile and induced drag components for the clean and iced wing. The lift coefficient and drag coefficients were determined from wake survey data. The results show that, for a given C_L, the profile drag of the iced wing was significantly higher than for the clean wing. Over the range of C_L's shown the ice shape more than doubled the profile drag. This was expected given the large region of separated flow behind the ice shape seen in the oil flow visualization. It can also be seen in Fig. 7 that as C_L was increased, the profile drag of the iced wing increased much faster than for the clean wing. This rapid rise in profile drag was due to the increasing size of the leading-edge vortex on the iced wing as seen in Fig. 5. The induced drag was not significantly influenced by the presence of the ice shape. Figure 7 shows that the curves of C_L vs. C_{Di} of the clean and iced wing almost exactly coincided for $C_L < 0.55$. As a result, for a given C_L below iced wing stall, the increase in drag due to the ice shape was nearly entirely due to a rise in the profile drag. Figure 7 also shows that the majority of the drag rise at stall, for the clean and iced wing, was due to a rise in the profile drag. These results show that the primary effect of the ice on the drag was to increase the axial momentum loss as opposed to changing the amount of streamwise vorticity shed into the wake.

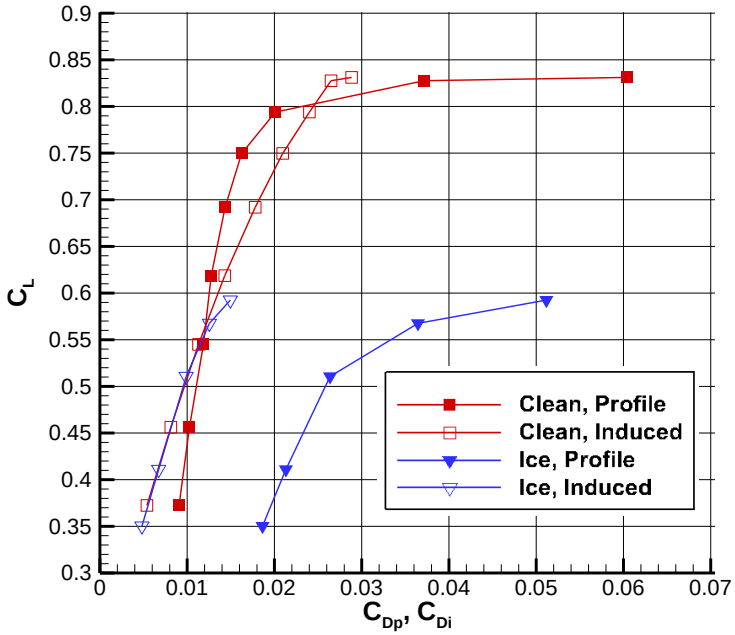

Fig. 7 Components of drag for clean and iced wing. Re = $6x10^5$.

Figure 8 shows the spanwise distributions of the lift coefficient as well as the total drag, profile drag and induced drag coefficients for the clean and iced wing at $\alpha = 4.4^o$. Note that because wake surveys were only performed at a few angles of attack, it was not possible to compare lift and drag distributions of the clean and iced wings for the same C_L. At $\alpha = 4.4^o$, total C_L and C_D of the clean wing measured by the force balance were 0.522 and 0.027 respectively. For the iced wing at $\alpha = 4.4^o$, total C_L and C_D were 0.5070 and 0.042 respectively. Over nearly the entire span, the local lift coefficient was decreased, Fig. 8a, and the drag coefficient was increased, Fig. 8b, by the presence of the ice shape. It can also be seen that the largest differences in the local lift and drag coefficients occurred outboard of approximately midspan. This was a consistent trend seen for all angles of attack; when the ice was present the local aerodynamic penalties were greater on the outboard sections of the wing. As discussed above this was also seen in the oil flow images, Fig. 5, where the size of the recirculation region occupied a larger percentage of the chord on the outboard sections of the wing. It was seen in Fig. 3 that the size of the ice shape relative to the local chord was much larger for the outboard sections of the wing, and this likely plays in important role in the ice shape having a larger effect near the tip. In addition to the relative size of the ice shape the spanwise pressure gradient may be another factor that led to increased performance degradation for the outboard sections of the wing. The spanwise flow, which results from the spanwise pressure gradient, acts as a form of boundary layer suction for the inboard sections making these sections more resistant to separation and possibly promoting reattachment of the separated shear layer.[18]

Figures 8c and 8d show spanwise distributions of the profile and induced drag. Consistent with Fig. 7, all of the increase in drag due to the ice shape was a result of an increase in the profile drag. Figure 8d shows that differences in the induced drag distributions of the clean and iced wing were negligible along most of the span except near the tip. Near the tip of the clean wing the change in the lift with respect to the spanwise location was much larger than for the iced wing indicating the clean wing was shedding more vorticity into the wake. The 5HP wake surveys of Diebold et. al.[9] showed that the tip vortex of the clean wing was much stronger than the tip vortex of the iced wing for nearly identical lift coefficients. This resulted in a large peak in the local induced drag of the clean wing near the tip. In addition, the large axial velocity deficit within the tip vortex resulted in peaks in the local profile drag coefficient near the tip for both the clean and iced wings. The axial velocity deficit within the iced wing vortex was larger due to the entrainment of separated flow into the vortex. This resulted in a larger profile drag coefficient near the tip of the iced wing.

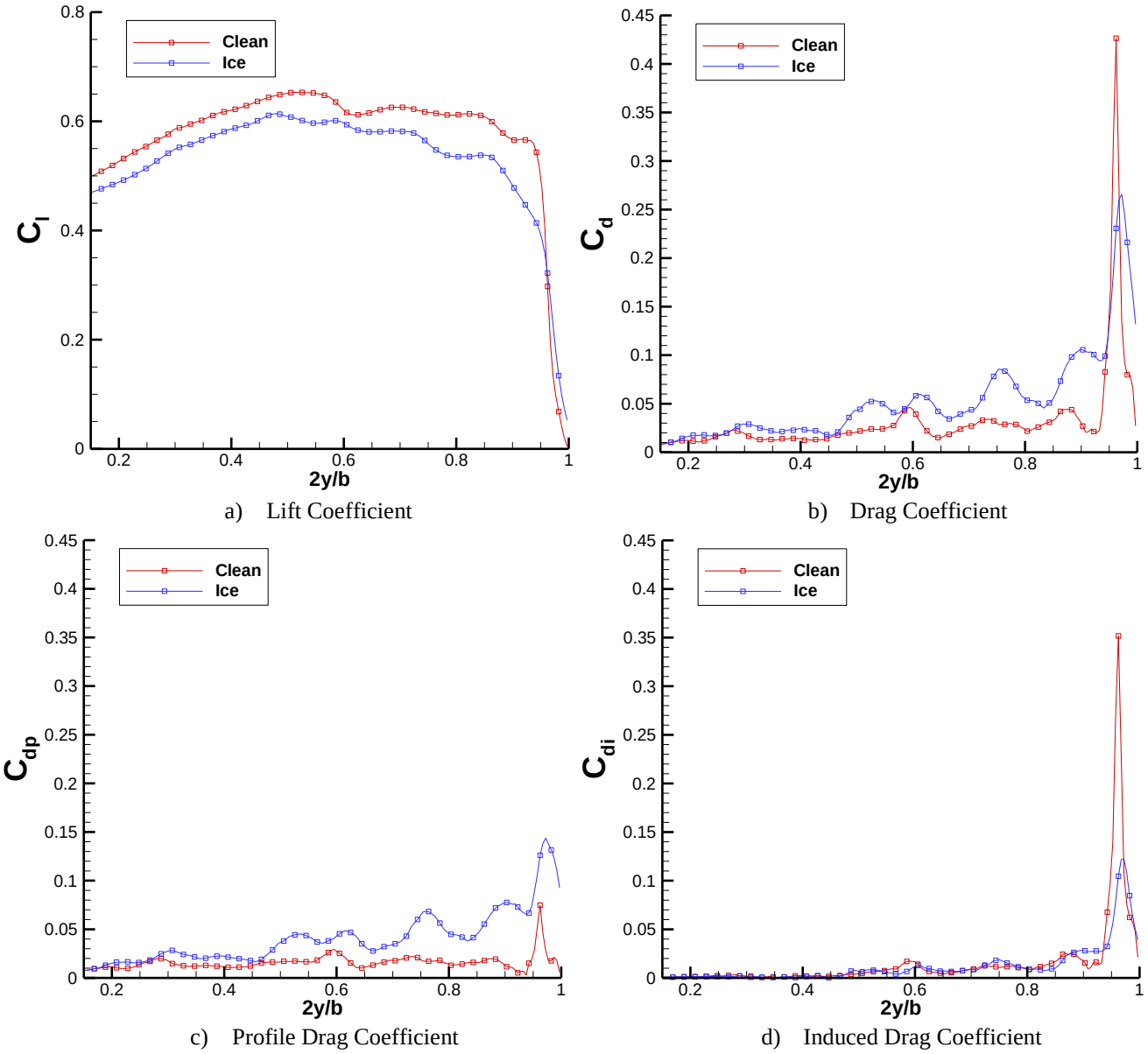

Fig. 8 Spanwise distributions of a) Lift coefficient, b) Drag coefficient, c) Profile drag coefficient and d) Induced drag coefficient for the clean and iced wing at α = 4.4°. Re = 6x10^5.

The distributions of total, profile and induced drag, Figs. 8b, c and d, show several local peaks along the span. These peaks were especially prominent for the iced wing. Figure 9 shows how the peaks in the profile drag coefficient of the iced wing at α = 4.4° corresponded to regions of concentrated axial velocity deficit in the wake. The contours in the wake represent normalized axial velocity while the vectors represent the crossflow velocity. Similarly, peaks in the induced drag coefficient corresponded with regions of concentrated axial vorticity as shown in Fig. 10. The peaks in profile and induced drag occurred at the same location. In addition, examining Fig. 8a shows that at these same spanwise locations there is a decrease in the local lift coefficient. This indicates a change in the local circulation occurred explaining the concentrated regions of shed vorticity. It is not surprising that peaks in the drag distributions corresponded to features in the wake since the distributions were determined from wake data, but these figures indicate that something is occurring on the surface of the wing that sheds vorticity and generates a loss of axial momentum.

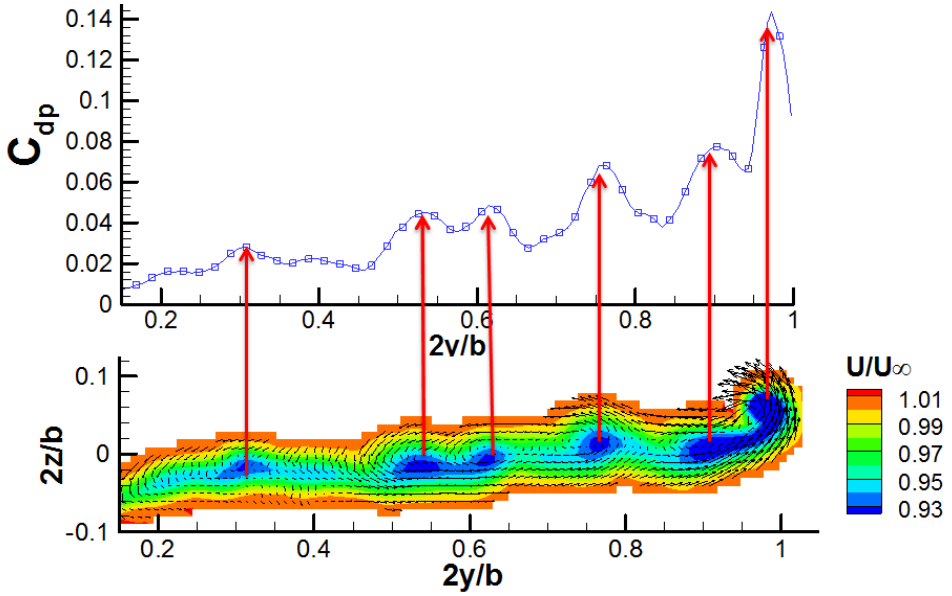

Fig. 9 Correlation between regions of concentrated axial velocity deficit and local peaks in profile drag for the iced wing. α = 4°, Re = 6x10^5

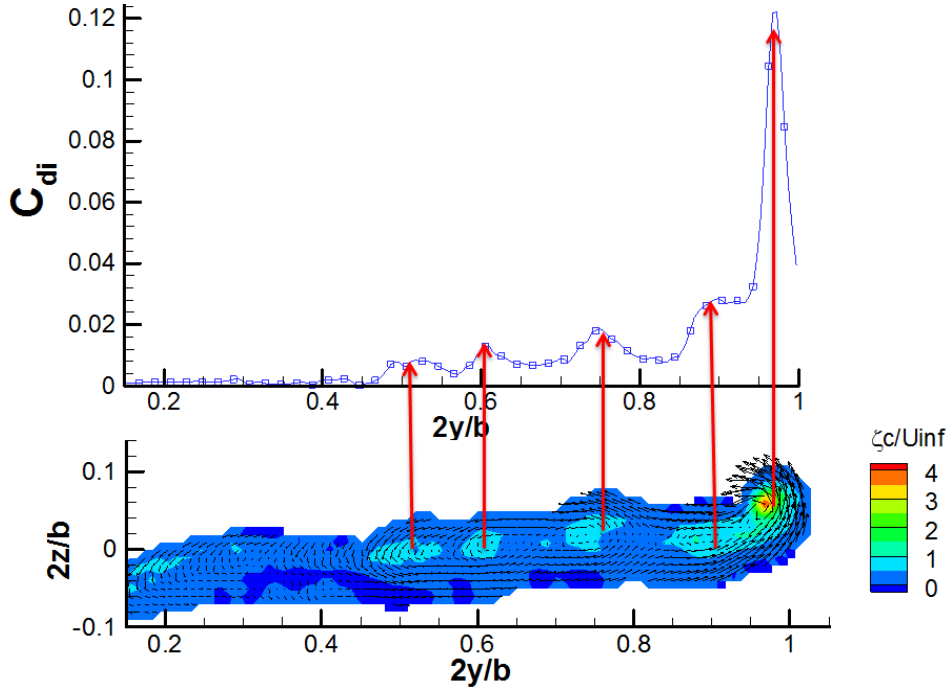

Fig. 10 Correlation between regions of concentrated axial vorticity and local peaks in induced drag for the iced wing. α = 4°, Re = 6x10^5

Figure 11 is an attempt to relate features in the wake, which correspond to peaks in the local drag coefficients, of the iced wing at $\alpha = 4.4^{\circ}$ to features seen in the oil flow. It can be seen that several of the concentrations of low axial velocity in the wake corresponded with local maxima in the size of the leading-edge vortex. This was observed for all angles of attack for the iced wing, see Diebold.[17] While it is unknown exactly why the size of the leading-edge vortex changed at these locations, it was clear that this had an effect on the local aerodynamic performance. When a local maxima in the leading-edge vortex was encountered, the local aerodynamics of this section were affected more than the neighboring sections because of the larger percentage of the chord being affected by the separated flow. This resulted in a local rise in the pressure drag which is seen as the concentration in low axial velocity in the wake and a peak in profile drag. In addition, because of the larger separated region, the lift at these sections decreased slightly resulting in vorticity being shed into the wake and a peak in induced drag.

The low axial velocity region near $2y/b = 0.6$, and the corresponding local maxima in drag, was observed in all of the wakes for both the clean and iced wing below stall but did not appear to correlate with any feature seen in the oil flow. It is possible that this feature may have originated from the lower surface.

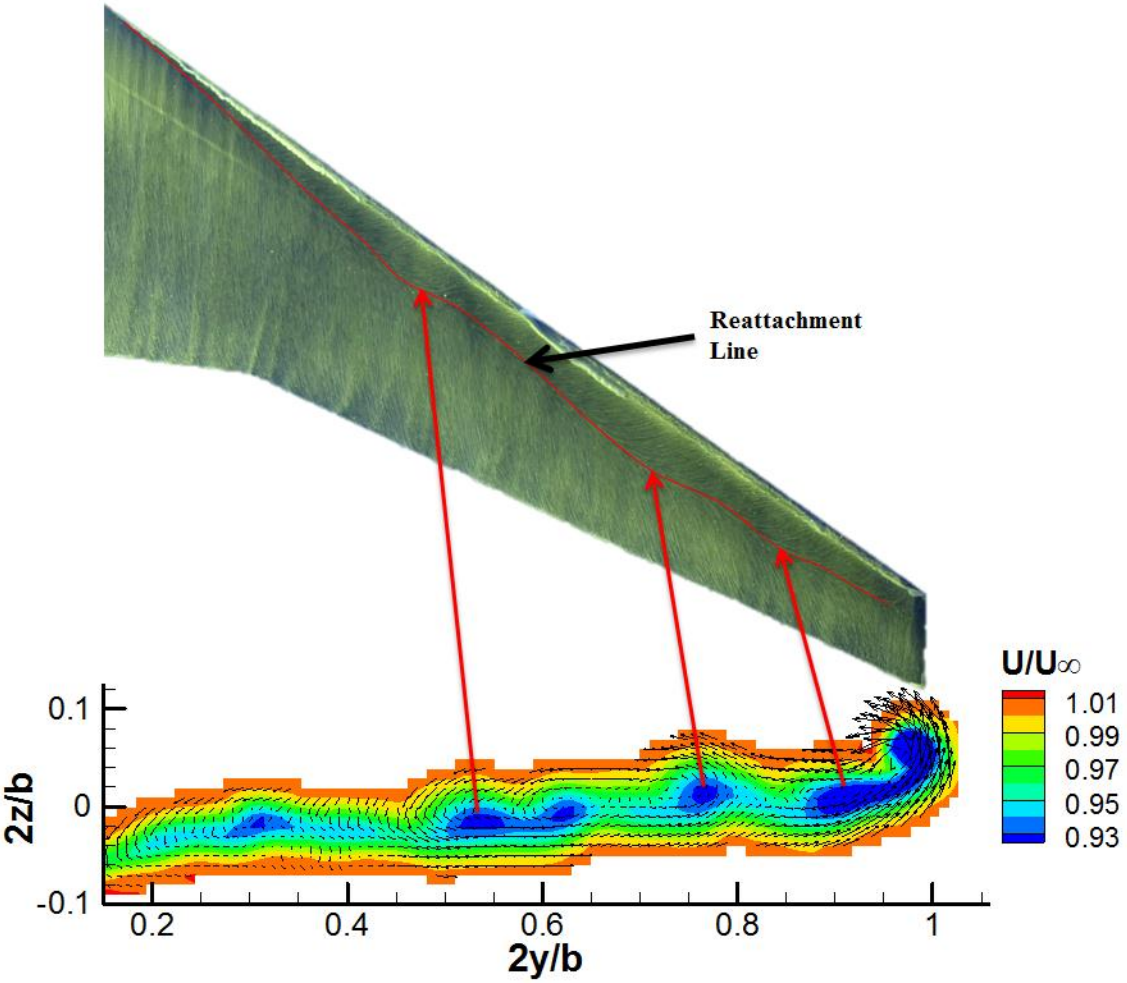

Fig. 11 Correlation between features in the wake and the surface oil flow for the iced wing. $\alpha = 4^{\circ}$, Re = $6x10^5$

The wake survey results were also used to investigate the effects of stall on the clean and iced wing. Figures 12a and 12c compare the spanwise distributions of the clean wing lift and drag for an angle of attack just prior to stall ($\alpha = 8.6^{\circ}$) and just after stall ($\alpha = 10.7^{\circ}$), Figs. 12b and 12d compare the distributions of lift and drag for the iced wing just prior to stall ($\alpha = 5.5^{\circ}$) and just after stall ($\alpha = 6.5^{\circ}$). Note the difference in scales for the clean wing figures and iced wing figures. Since the stalling angles of attack are sufficiently different between the clean and iced cases a direct comparison is not as useful.

Recall from the oil flow images, Figs. 4 and 5, that stall of the clean and iced wing occurred when flow on the outboard stations failed to reattach. The separated flow rolled up to form a leading-edge vortex which was shed into the wake at approximately 2y/b = 0.6. The flow inboard of the vortex remained attached while outboard the flow on the surface was fully reversed. The stalled wing flowfields are described in more detail by Diebold et. al.[9] The effects on the lift distribution can be seen in Figs. 12a and b. For both the clean and iced wing the lift on the inboard sections continued to increase through stall, and the lift on the outboard sections decreased significantly due to the separated flow. These results explain the behavior of the lift curve after stall as seen in the force balance measurements in Fig. 6. For both the clean and iced wing the lift did not decrease as a result of stall. For the clean wing, the lift was nearly constant as the angle of attack continued to increase, while for the iced wing the lift continued to increase but the slope of the curve had decreased. The wake survey results show that the inboard sections of the wing are able to compensate for the loss of lift produced by the outboard sections, and prevent the lift from decreasing.

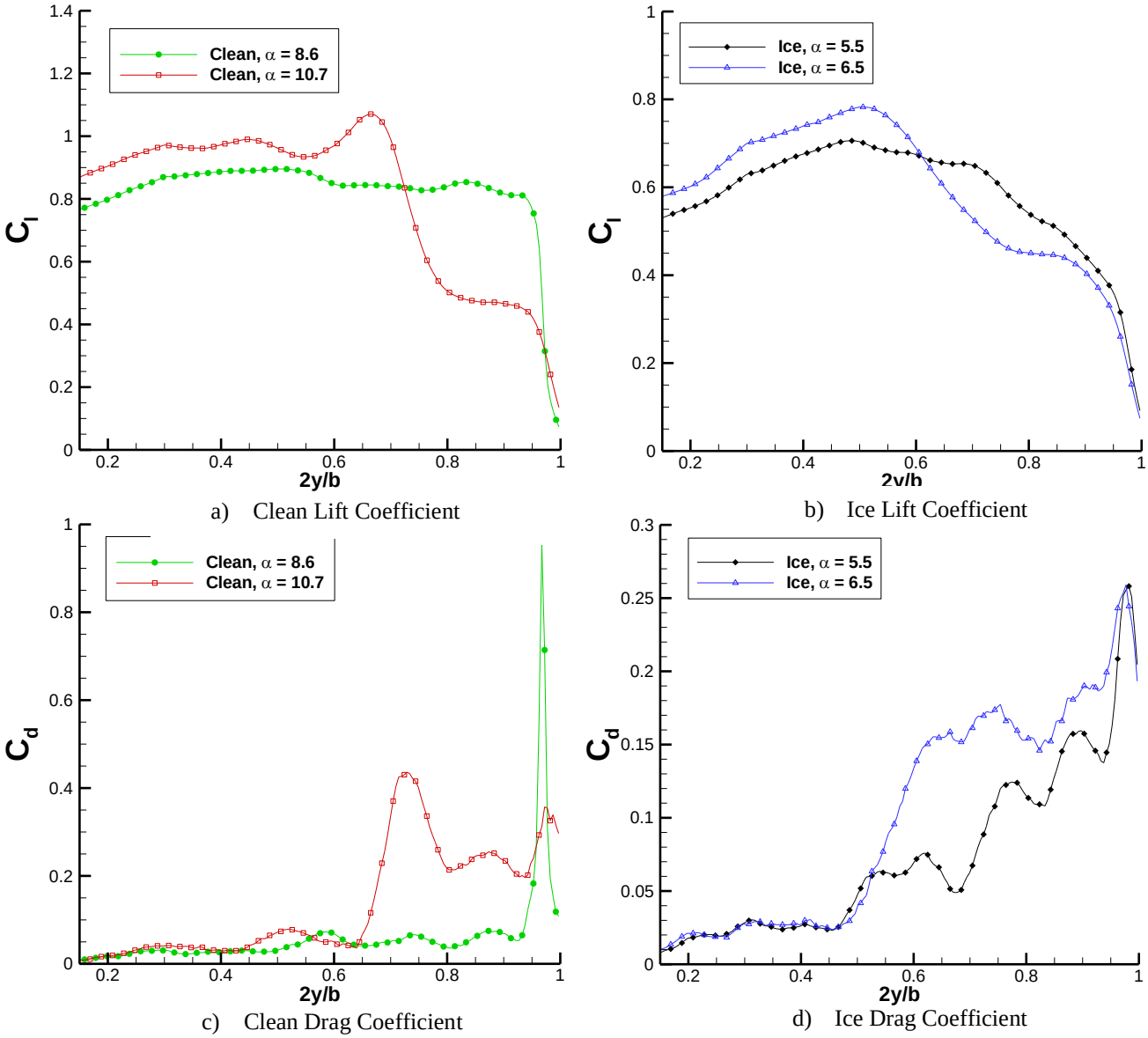

a) Clean Lift Coefficient

b) Ice Lift Coefficient

c) Clean Drag Coefficient

d) Ice Drag Coefficient

Fig. 12 Comparison of pre and post stall spanwise distributions of a) Clean wing lift coefficient, b) Ice wing lift coefficient, c) Clean wing drag coefficient and d) Ice wing drag coefficient. Re = 6x10^5.

While not shown here, the force balance measurements also showed an increase in the pitching moment resulting from stall, see Diebold et. al.[9] The mean aerodynamic chord of the model was located at roughly 2y/b = 0.40. Therefore, due to the wing sweep, the sections of the wing that stalled were behind the quarter chord of the mean aerodynamic chord as seen in Figs. 12a and b. This resulted in an increased, nose up, pitching moment for the model as a result of stall.

The effects of stall on the drag coefficient can be seen in Figs. 12c and d. Inboard of the separated region the distribution of the drag coefficient was relatively unchanged for both the clean and iced wing; however, there was a significant increase in the drag of the outboard sections where the flow had separated. Figures 13a and c show the spanwise distribution of profile and induced drag on the clean wing pre and post stall, and Figs. 13b and d show the corresponding distributions for the iced wing. As was seen in Fig. 7, the drag rise due to stall was primarily due to an increase in the profile drag for both the clean and iced wings. The surface flowfield and wake flowfield of the stalled wings were discussed in detail by Diebold et. al.[9] where it was shown that the separated outboard sections resulted in a large momentum deficit region in the wake.

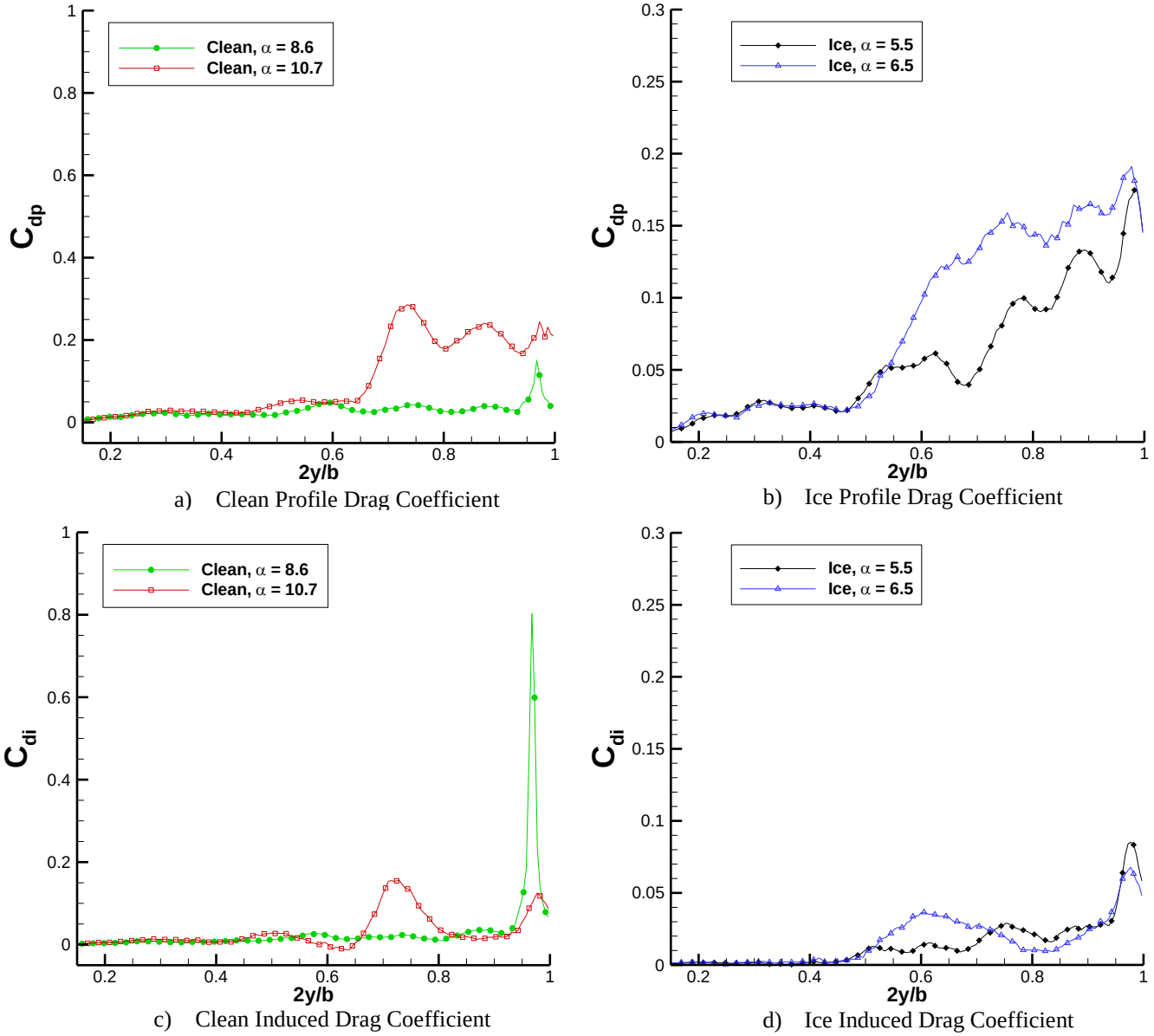

Fig. 13 Comparison of pre and post stall spanwise distributions of a) Clean wing profile drag coefficient, b) Ice wing profile drag coefficient, c) Clean wing induced drag coefficient and d) Ice wing induced drag coefficient. Re = 6x10^5.

Figure 7 showed that the total induced drag, unlike the profile drag, did not undergo a rapid increase as the wing stalled. Figures 13c and d show that although the total induced drag did not change significantly the distribution of induced drag was altered. The separated flow on the outboard sections led to a reduction in the strength of the tip vortex resulting in a decreased contribution to the induced drag from the tip section of the wing. This was especially apparent for the clean wing. Once the wing stalled, the major contributor to induced drag was the leading-edge vortex shed from inboard of the tip. It is also interesting to point out, in Fig. 13c from approximately $2y/b = 0.6$ to 0.65 the induced drag of the clean wing was negative. The rotation of the leading-edge vortex induced an upwash on this section of the wing tilting the force vector forward, resulting in a region of local thrust. This thrust from the induced velocities was not large enough to overcome the local pressure drag and the total drag contribution of this spanwise section was still positive.

5.0 Conclusion

Previous surface pressure and flow visualization experiments[4,9] have shown that the aerodynamics of swept wings with ice are highly three dimensional and complex. When investigating the performance effects of the ice a force balance is only capable of providing the total lift and drag. It cannot provide any information regarding the breakdown of the different drag components, nor can it provide any information regarding the spanwise variation in the local performance characteristics of the wing although the pitching moment can indicate tip stall. Surface oil flow visualization provides insight into the spanwise variation of the performance but does not generate any quantitative information.

This paper utilized five-hole probe measurements and a wake survey analysis to determine how the ice effects the different drag components and how the local aerodynamics of the wing were influenced by the ice. Drag decomposition showed that the leading-edge ice significantly increased the profile drag of the wing while the induced drag was reduced slightly. Examining the surface oil flow images, it was determined that this rise in profile drag was due to the large leading-edge vortex that resulted from flow separation at the tip of the ice shape.

The spanwise distributions of lift and drag showed that for this particular ice shape, the outboard sections of the wing suffered greater performance degradation than the inboard sections. Decreases in the local lift coefficient and increases in the local drag coefficient were larger on the outboard sections of the wing. This was a result of the size of the ice shape relative to the local chord as well as the fundamental aerodynamics of swept wings such as the spanwise pressure gradient. It was also shown that it is possible to relate features in the spanwise distributions of lift and drag to the features seen in the surface oil flow visualization. This provides a more complete understanding of how the ice influenced the wing.

As the clean and iced wing stalled, the surface oil flow showed a large leading-edge vortex was shed into the wake resulting in two distinct regions on the wing. Inboard of the leading-edge vortex the flow remained attached while outboard of the vortex the flow was fully separated. The spanwise distributions of lift showed that while the wing stalled, the lift on the inboard sections continued to increase and compensated for the loss of lift on the outboard sections preventing a decrease in lift due to stall.

Information about the effects of ice on the local aerodynamics of a wing can be very valuable from an aircraft safety point of view. Lynch and Khodadoust[1] stress the importance of the critical spanwise location along the wing. The location on the wing that is most sensitive to ice. The wake survey method can help identify critical regions along the wing.

Acknowledgements

This work was supported under grant DOT FAA 10-G-004. The authors would like to acknowledge the contribution of their technical monitor Dr. Jim Riley of the FAA Technical Center. We would also like to thank Marianne Monastero and Abigail Atkinson for assisting with various experiments. Thanks are also due to Joe Bottalla and Andrew Mortonson for their work on the design of the swept wing model.

References

[1] Lynch, F.T. and Khodadoust, A., "Effects of Ice Accretions on Aircraft Aerodynamics," *Progress in Aerospace Sciences*, Vol. 37, p. 669-767, 2001.

[2] Bragg, M.B., Broeren, A.P., and Blumenthal, L.A., "Iced-Airfoil Aerodynamics," *Progress in Aerospace Sciences* Vol. 41, p. 323-362, 2005.

[3] Broeren, A.P., Bragg, M.B., Addy, H.E., Lee, S., Moens, G. and Guffond, D., "Effect of High-Fidelity Ice Accretion Simulations on Full-Scale Airfoil Performance," *Journal of Aircraft*, Vol. 47, No. 1, January-February 2010.

[4] Papadakis, M., Yeong, H.W. and Wong, S.C, "Aerodynamic Performance of a Swept Wing with Ice Accretions," AIAA 2003-0731

[5] Vargas, M., Papadakis, M., Potapczuk, M.G., Addy, H.E. Jr., Sheldon, D., and Giriunas, J., "Ice Accretions on a Swept GLC-305 Airfoil." SAE 02GAA-43, SAE General Aviation Technology Conference and Exhibition, Wichita, KS, Apr. 2002, Also NASA/TM-2002-211557, Apr. 2002.

[6] Papadakis, M., Alansatan, S., and Yeong, H.W., "Aerodynamic Performance of a T-Tail with Simulated Ice Accretions," AIAA Paper 2000-0363, Jan. 2003.

[7] Broeren, A.P., Lee, S., Shah, G.H. and Murphy, P.C., "Aerodynamic Effects of Simulated Ice Accretion on a Generic Transport Model," SAE Technical Paper 2011-38-0065

[8] Bragg, M.B., Kerho, M.F., and Khodadoust, A., "LDV Flowfield Measurements on a Straight and Swept Wing with a Simulated Ice Accretion," AIAA 1993-0300

[9] Diebold, J.M., Monastero, M.C. and Bragg, M.B., "Aerodynamic of a Swept Wing with Ice Accretion at Low Reynolds Number," AIAA 2012-2795

[10] Hackett, J.E. and Sugavanam, A., "Evaluation of a Complete Wake Integral for the Drag of a Car Like Shape," SAE Paper No. 840577, February 1984

[11] Brune, G. W., "Quantitative Low Speed Wake Surveys," *Journal of Aircraft* Vol. 31, No. 2, 1994.

[12] Kusunose, K,. "Development of a Universal Wake Survey Data Analysis Code," AIAA 1997-2294.

[13] Betz, A., "A Method for the Direct Determination of Profile Drag," ZFM, Vol. 16, pp.42, 1925

[14] Maskell, E.C., "Progress Towards a Method for the Measurement of the Components of the Drag of a Wing of Finite Span," RAE Technical Report 72232, 1972.

[15] Vassberg, J.C., DeHaan, M.A., Rivers, S.M. and Wahls, R.A., "Development of a Common Research Model for Applied CFD Validation Studies," AIAA 2008-6929

[16] Potapczuk, M.G., Papadakis, M.J., and Vargas, M., "LEWICE Modeling of Swept Wing Ice Accretions," AIAA 2003-0730

[17] Diebold, J.M., "Aerodynamics of a Swept Wing with Leading-Edge Ice at Low Reynolds Number" M.S. Thesis, Department of Aeronautical and Astronautical Engineering, University of Illinois, Urbana, IL. August 2012

[18] Hoerner, S.F., Fluid-Dynamic Lift, Hoerner Fluid Dynamics, Brick Town, NJ, 1975.